ACS OMEGA

Article

http://pubs.acs.org/journal/acsodf

Making a Supertough Flame-Retardant Polylactide Composite through Reactive Blending with Ethylene-Acrylic Ester-Glycidyl Methacrylate Terpolymer and Addition of Aluminum Hypophosphite

Shuang Li,[†] Liang Deng,[†] Cui Xu, Qianghua Wu, and Zhigang Wang*

CAS Key Laboratory of Soft Matter Chemistry, Department of Polymer Science and Engineering, Hefei National Laboratory for Physical Sciences at the Microscale, University of Science and Technology of China, Hefei, Anhui 230026, P. R. China

Supporting Information

ABSTRACT: Biocompatible and biodegradable polylactide (PLA) composites with supertough mechanical property and sufficient flame retardancy were fabricated by employing a facile approach involving reactive blending of PLA and ethylene-acrylic ester-glycidyl methacrylate terpolymer (EGMA), with the addition of aluminum hypophosphite (AHP) as an effective flame retardant. In consideration of the balance between mechanical property and flame retardancy, the optimal formula was taking a PLA/EGMA 80/20 blend (supertough STPLA) as the matrix and adding 20 wt % of AHP (relative to the mass of STPLA) as the flame retardant, coded as STPLA/20AHP. The mechanical property test showed that for STPLA/20AHP the elongation at break was increased by about 22 times and the notched Izod impact strength was enhanced by approximately 11 times as compared to those for neat PLA. The flame-retardant property test showed that for STPLA/20AHP the limiting oxygen index value reached 26.6% and the UL-94 V0 rating test was passed. Thermogravimetric analysis, microscale combustion calorimetry, and cone calorimeter were further applied to reveal the thermal stability and combustion behaviors of STPLA/*x*AHP, respectively, where *x* indicated the mass content of AHP in percentage. The phase separation morphology, dispersion of AHP particles in STPLA matrix, and fracture surfaces and char residues after flame burning were examined by phase contrast optical microscopy and scanning electron microscopy, respectively, which helped comprehend the results obtained from the mechanical property and flame retardancy tests. The supertough STPLA/*x*AHP, with sufficient flame retardancy as prepared in this work, could have a potential for engineering applications.

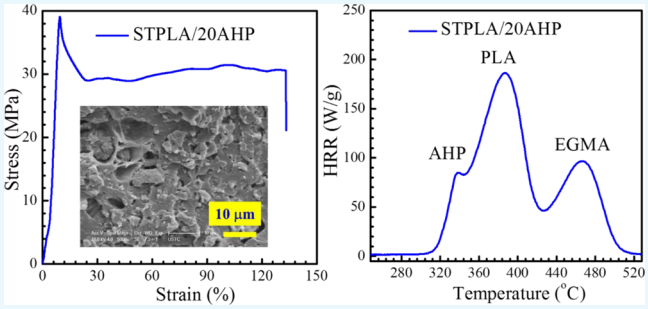

1. INTRODUCTION

Polylactide (PLA), as a promising bio-based polymer, has been paid much attention.[1−3] Due to its excellent properties, PLA has been widely used in many fields, such as the packaging industry, household engineering, and biomedical devices. The applications of PLA might further be expanded to automotive materials, electronic appliances, and transportation.[4,5] However, its mechanical and flame-retardant properties are insufficient for use in these burgeoning applications.

Due to a low entanglement density and high value of the characteristic ratio, neat PLA possesses inherent brittleness, with the elongation at a break of less than 10% and notched Izod impact strength of about 2 kJ/m^2.[6] Besides, the poor fire resistance of PLA also restricts its further application and development in the industrial fields mentioned above. Therefore, for the burgeoning applications, simultaneously improving its mechanical properties, especially notched Izod impact strength, and flame retardancy remains the main challenge to be resolved.

Researchers attempted various methods to improve the flame retardancy of PLA materials in the past years.[7−13] In particular, inorganic phosphorus-based intumescent flame retardants have been used as flame-retardant additives for PLA and some effective flame-retardant systems have been developed as well.[14−22] Zhan et al. synthesized an intumescent flame retardant, spirocyclic pentaerythritol bisphosphorate disphosphoryl melamine (named SPDPM), and the PLA sample with 25 wt % loading of SPDPM reached UL-94 V0 rating and had a high limiting oxygen index (LOI) value of 38 vol %.[23] Stoclet et al. reported that addition of 17 wt % halloysite decreased the peak intensity of the heat release rate (PHRR) of a PLA/halloysite nanocomposite by 40% as compared to that of PLA control.[19] Réti et al. introduced lignin and starch into an ammonium polyphosphate (APP)/bioresources system for improving the flame retardancy of PLA.[24] Their results showed that the flame-retarded PLA achieved the UL-94 V0 rating at a loading of 40 wt % of the flame retardant. Aluminum hydroxide,[25] expanded graphite,[26] and *β*-cyclodextrin[27] were also used as other flame-retardant additives in the past decades. However, the obvious disadvantage of the loading of these

Received: February 11, 2017
Accepted: April 25, 2017
Published: May 8, 2017

DOI: 10.1021/acsomega.7b00162
ACS Omega 2017, 2, 1886−1895

flame retardants in such high contents is that the mechanical properties of the PLA materials could diminish significantly.

Hence, with an aim of keeping a balance between the flame retardancy and mechanical properties of PLA, reactive blending of the flame-retardant PLA with the reactive polymer elastomer has been regarded as an effective approach to improve the toughness. Reactive blending is a cost-effective technique through which compatibilizers are produced in situ by chemical reactions at the interface during mixing that has been widely utilized to improve the toughness of PLA.[28−31] For example, Oyama prepared high-performance PLA blends by reactive blending of PLA with ethylene-acrylic ester-glycidyl methacrylate terpolymer (EGMA), showing an increase of over 50 times in the impact strength than that of neat PLA.[32] Fang et al. prepared supertough PLA materials through in situ reactive blending of PLA with poly(ethylene glycol)-based diacrylate monomer (PEGDA), showing improvements by a factor of 20 in the tensile roughness and a factor of 26 in the notched Izod impact strength at the optimum CPEGDA content.[31] Liu et al. reported on the preparation of supertough PLA ternary blends, consisting of PLA, elastomeric ethylene-butyl acrylate-glycidyl methacrylate terpolymer (EBA-GMA), and zinc ionomer of ethylene-methacrylic acid copolymer.[33,34] Effective interfacial reactions between the epoxy groups of EBA-GMA and the terminal groups of PLA were thought to be responsible for significant increases in the notched Izod impact strength of the PLA materials. Some other flexible polymers with reactive functional groups have also been studied to improve the toughness of PLA through interfacial reactions.[35−38]

The effective methods for preparing supertough PLA materials have shed light on the preparation of PLA materials with a balance between their mechanical property and flame retardancy. In this work, we have employed a facile approach for the preparation of PLA composites with sufficient mechanical performance and flame retardancy. A detailed analysis of the phase structure and morphology has been performed to reveal the achieved balance between the mechanical and flame-retardant properties. To the best of our knowledge, the approach to preparing supertough PLA composites with sufficient flame retardancy in this work might pave the way to its utilization in large-scale commercial applications.

2. RESULTS AND DISCUSSION

2.1. Supertough STPLA/*x*AHP. PLA, derived from renewable resources as a promising bio-based polymer, has attracted much attention because of its biodegradability, biocompatibility, high mechanical strength, and excellent processability.[39−42] However, the inherent poor toughness of PLA significantly limits its use in a wide range of applications, such as in automotive and packaging industries.[43,44] The reactive blending of PLA and EGMA might provide toughness improvement;[45] certain multiphase blend systems on the basis of PLA/EGMA matrix with improved mechanical or thermal properties have been reported.[43,46,47] It has been predicted that the glycidyl groups with high concentration (8%) in EGMA can react with carboxyl and hydroxyl in PLA to form an effective interfacial layer, which helps to improve greatly the toughness of PLA materials.

Figure 1 shows the typical nominal stress−strain curves for PLA/EGMA 80/20 blend (STPLA) and PLA/EGMA composites (STPLA/*x*AHP) with different flame-retardant aluminum hypophosphite (AHP) contents. It can be seen

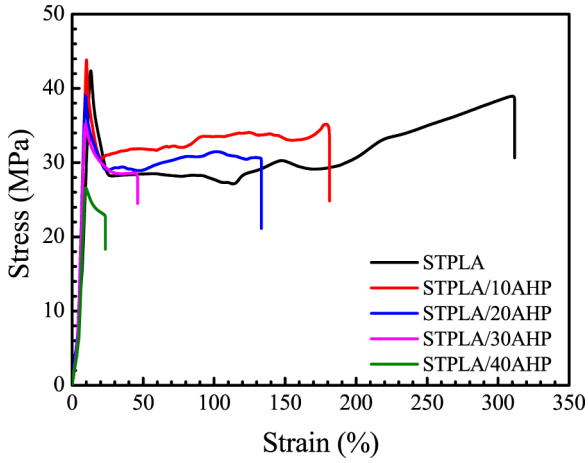

Figure 1. Typical nominal stress−strain curves for STPLA (PLA/EGMA 80/20 blend) and its composites (STPLA/*x*AHP) with different AHP contents.

that PLA/EGMA 80/20 blend (STPLA) displays excellent tensile toughness with an elongation at break of 310%, whereas the elongation at break for neat PLA is just around 5.7%.[31] Therefore, the improvement by 53 times in the elongation at break demonstrates that PLA/EGMA 80/20 blend (STPLA) can be considered as a supertough PLA material.[31] With increasing content of the added flame retardant, AHP into STPLA, the elongation at break for STPLA/*x*AHP gradually decreases. Nevertheless, for the flame-retardant AHP contents of 10 and 20 wt % the elongations at break are still higher than 130%, which infers that STPLA/10AHP and STPLA/20AHP are still supertoughened PLA composites for application purpose. It is further noticed that even when the flame-retardant AHP content is 30 wt % the elongation at break for STPLA/30AHP still reaches 45%, which is far beyond that for neat PLA.

The changes of yield strength, tensile modulus, tensile toughness, and notched Izod impact strength as functions of AHP content for STPLA/*x*AHP are shown in Figure 2. As can be seen from Figure 2a, the incorporation of AHP rigid particles as a flame retardant in STPLA can remedy certain loss in yield strength or tensile modulus because the loss results from the introduction of the soft elastomer EGMA. For example, when AHP of 10 wt % is added in, the yield strength and tensile modulus for STPLA/10AHP are 44 and 736 MPa, while these values for STPLA are 42 and 568 MPa, respectively. Further increase of the AHP content results in a decrease in both the variables. Nonetheless, the tensile moduli of STPLA/*x*AHP are still higher than that of STPLA even when the AHP content reaches 30 wt %. As seen from Figure 2b, both the notched Izod impact strength and tensile toughness continuously decrease with increasing AHP content due to the rigid nature of AHP particles. Although the notched Izod impact strength and tensile toughness deteriorate with the addition of AHP, STPLA/*x*AHP is superior to neat PLA. For example, the notched Izod impact strength for STPLA/40AHP is 5.7 kJ/m^2, nearly three times of that for neat PLA (1.9 kJ/m^2). It will be presented in a later section that there is no need to pursue the highest AHP content of 40 wt % for flame-retardant purpose; as a matter of fact, an AHP content of 20 wt % is sufficient for effective flame retardancy from the application viewpoint. The notched Izod impact strength is about 22 kJ/m^2 for STPLA/20AHP, which is nearly 12 times of that for neat PLA. In short,

DOI: 10.1021/acsomega.7b00162
ACS Omega 2017, 2, 1886−1895

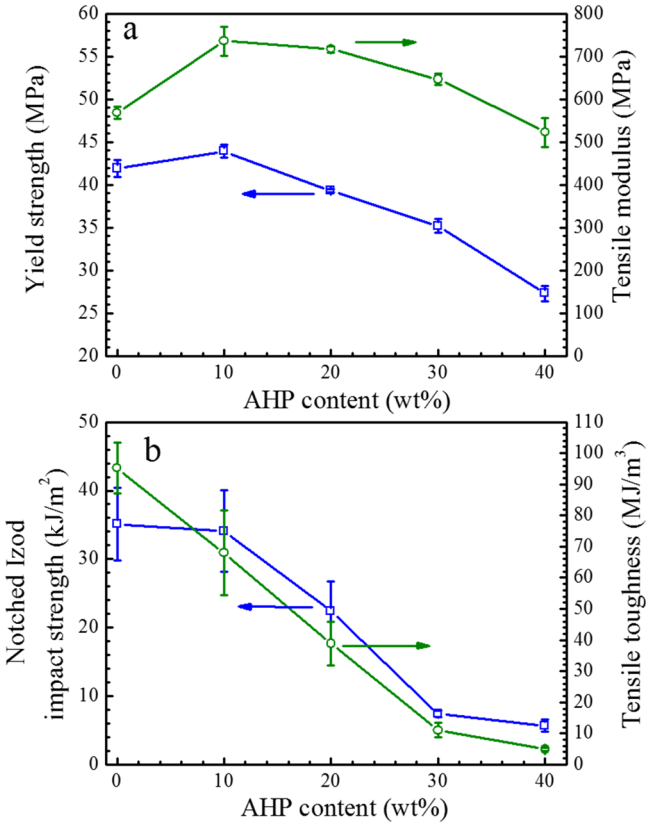

Figure 2. Changes in yield strength and tensile modulus (a) and notched Izod impact strength and tensile toughness (b) as functions of flame-retardant AHP content for STPLA/*x*AHP with different AHP contents. Note that the tensile toughness values were determined from the areas under the nominal stress−strain curves.

the STPLA matrix provides a broad platform for the incorporation of flame-retardant AHP, and the addition of AHP can make some remedies to the rigidity sacrifice resulting from the introduction of reactive soft elastomeric EGMA.

2.2. Flame Retardancy for STPLA/*x*AHP. AHP was reported as an effective flame retardant for polymers such as polyamide 6,6 and poly(ethylene terephthalate).[48,49] In this study, the LOI and Underwriters Laboratories UL-94 tests were performed to study the combustion behavior and determine the flammability standard for each STPLA/*x*AHP composite. The flammability test results are summarized in Table 1. Without addition of AHP, the LOI values for neat PLA and STPLA are 19.5 and 19.0%, respectively and ratings are not capable for these two samples according to the UL-94 rating. The elastomeric component EGMA contains a large fraction of ethylene co-monomer, which makes it more flammable than neat PLA. Figure S1 in the Supporting Information shows the HRR and total heat release (THR) curves for neat PLA, EGMA, and STPLA obtained from the cone calorimeter. EGMA has a PHRR of 2430 kW/m^2, whereas the PHRR value for neat PLA is 1100 kW/m^2. The THR values for EGMA are also much higher than those for neat PLA at the later stage of testing. This result demonstrates that EGMA is more flammable than neat PLA. When AHP of 10 wt % is added, the LOI value of STPLA/10AHP increases to 24.1%; however, STPLA/10AHP does not pass the UL-94 V0 rating test. Only when AHP of 20 wt % is incorporated, the LOI value of STPLA/20AHP increases to 26.6% and STPLA/20AHP also successfully passes the UL-94 V0 rating test. The study of introducing AHP into neat PLA by Tang et al. showed that the flame-resistant PLA composites reached the UL-94 V0 rating and LOI value increased to 28.5% with AHP loading of 20 wt %, consistent with our result.[50] However, their PLA/AHP composites had elongation at break of less than 4%, illustrating they were typically very brittle PLA materials. Both neat PLA and STPLA show a dripping phenomenon during the vertical-burning test. When AHP of 10 wt % is added into the STPLA matrix, dripping is partially inhibited. With an incorporation of AHP of 20 wt %, dripping is completely inhibited. By further increasing AHP contents (30 and 40 wt %), STPLA/*x*AHP composites have even higher LOI values, show antidripping performance, and pass the UL-94 V0 rating. In a comprehensive consideration of the mechanical property and flame retardancy, STPLA/20AHP apparently represents an optimal formula because it shows an elongation at break of above 120%, a notched Izod impact strength of higher than 20 kJ/m^2, and sufficient performance of flame retardancy. Such a balance between mechanical and flame-retardant properties can surely broaden the applications of PLA-based composites, especially in automotive and electronic equipment industries.

Table 1. LOI Values and UL-94 Test Results for Neat PLA, STPLA, and STPLA/*x*AHP with Different AHP Contents

sample code	LOI (%)	UL-94 rating	dripping during burning
neat PLA	19.5	NR	yes
STPLA	19.0	NR	yes
STPLA/10AHP	24.1	NR	yes
STPLA/20AHP	26.6	V0	no
STPLA/30AHP	28.4	V0	no
STPLA/40AHP	29.2	V0	no

[a]NR means "no rating".

2.3. Thermal Stability for STPLA/*x*AHP. The results from the UL-94 tests illustrate that AHP behaves as an effective flame retardant for the PLA material. To investigate the thermal stability behaviors of STPLA/*x*AHP, thermogravimetric analysis (TGA) measurements under nitrogen and air atmosphere were applied, respectively. Figures 3 and 4 show the mass loss and derivative mass loss curves from TGA measurements for neat PLA, STPLA, and STPLA/*x*AHP under nitrogen and air atmosphere, respectively. The corresponding thermal stability parameters are listed in Tables 2 and 3. As shown in Figures 3a and 4a, the onset decomposition temperatures, $T_{0.05}$ (defined as the temperature at which a mass loss of 5% occurs), for STPLA/*x*AHP are all lower than those for STPLA. As the AHP content increases, the $T_{0.05}$ values slightly decrease, indicating that the flame-retardant PLA composites have reduced thermal stability owing to the addition of AHP. As shown in Figures 3b and 4b, neat PLA displays a singular T_{max} at 385 °C under nitrogen atmosphere and at 372 °C under air atmosphere, and STPLA displays another T_{max} at around 469 °C under nitrogen atmosphere and at around 446 °C under air atmosphere. Note that T_{max} represents the temperature at the maximum mass loss rate. With an addition of AHP in STPLA, an additional lower T_{max} is seen at around 345 °C for nitrogen atmosphere and at around 339 °C for air atmosphere. It becomes obvious that the three T_{max}'s should correspond to the maximum mass loss rates for AHP, PLA, and EGMA components, respectively, running from the low value to the high ones. There are no obvious changes for the T_{max} of the PLA component with increasing AHP content under both nitrogen and air atmosphere. The

DOI: 10.1021/acsomega.7b00162
ACS Omega 2017, 2, 1886−1895

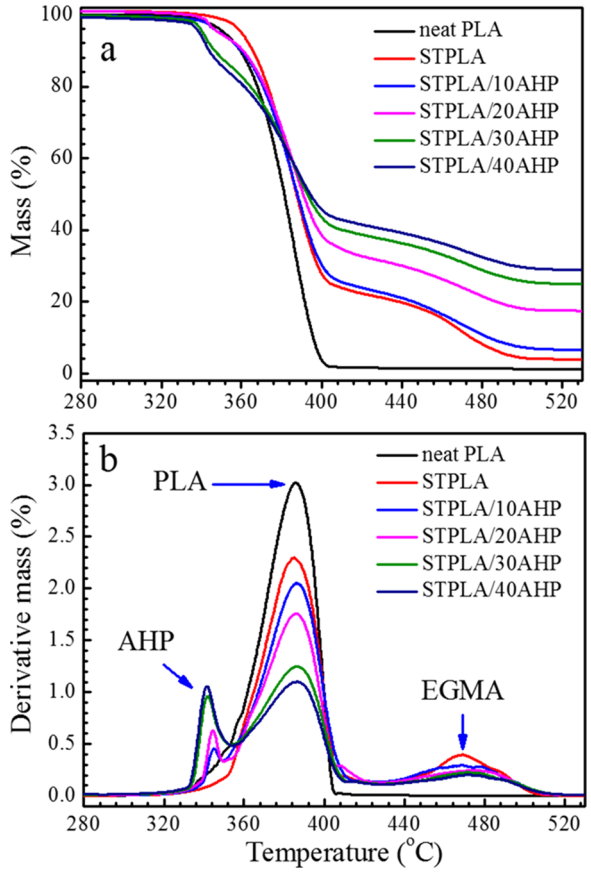

Figure 3. Mass loss curves (a) and derivative mass loss curves (b) from TGA measurements for neat PLA, STPLA, and STPLA/*x*AHP with different AHP contents under nitrogen atmosphere.

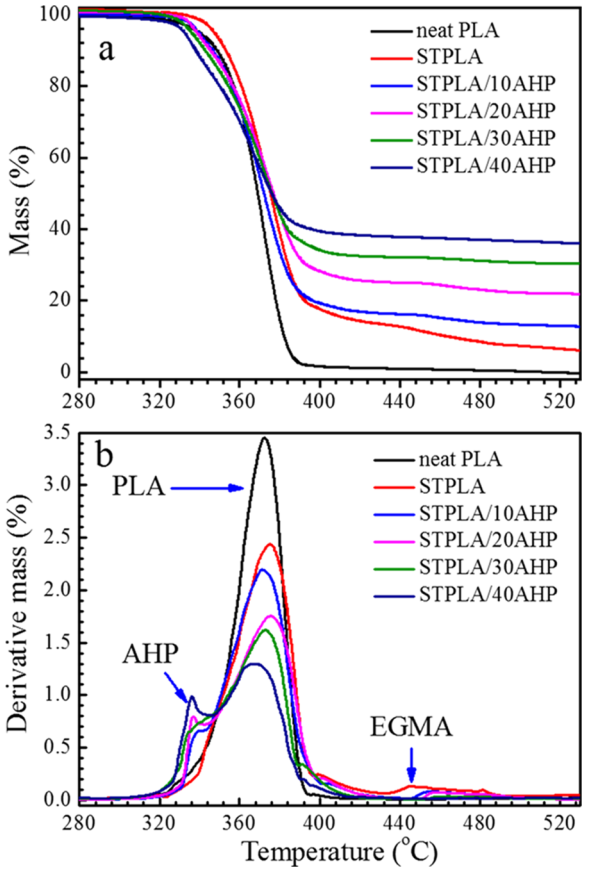

Figure 4. Mass loss curves (a) and derivative mass loss curves (b) from TGA measurements for neat PLA, STPLA, and STPLA/*x*AHP with different AHP contents under air atmosphere.

difference between the different testing atmospheres in this study lies in that all PLA materials show higher values of $T_{0.05}$ and T_{max} under nitrogen atmosphere than under air atmosphere, which is a common phenomenon for polymer thermal stability. For flame-retardant STPLA/*x*AHP, the thermal decomposition of AHP occurs at first, which can be confirmed by the lower $T_{0.05}$ values for STPLA/*x*AHP, the lowest T_{max} values for AHP in the composites, and the lower mass contents of residues than the initially added AHP contents in the composites. When thermal decomposition occurs in AHP, it produces phosphine (PH_3) and water (H_2O), which absorb heat and dilute oxygen in air to suppress combustion.[50] Besides, PH_3 reacts with oxygen to produce phosphoric acid (H_3PO_4), which acts as the acid source to promote carbonization of the polymer matrix and then helps form a carbon char on the sample surface to further separate oxygen from the sample to restrict further combustion.[50]

2.4. Flammability of STPLA/*x*AHP. For evaluating the combustion property of materials, microscale combustion calorimetry (MCC) is thought as one of the effective bench-scale measurement systems. MCC only requires milligrams of the samples for test. Basically, MCC uses an oxygen combustion calorimeter to measure the rate and amount of heat produced by complete combustion of the fuel gases generated during controlled heating of the sample.[51] Figure 5 shows the HRR curves obtained from the MCC test for neat PLA, STPLA, and STPLA/*x*AHP with different AHP contents. HRR is the most important parameter for evaluating the fire hazard of materials from the MCC test, in which a low HRR value indicates a low flammability with low full-scale hazards.[51] As can be seen from Figure 5, the PHRR is apparently different from PLA to STPLA as it is reduced from 372 W/g for PLA to 242 W/g for STPLA (a reduction of 35%). Another PHRR

Table 2. Thermal Stability Parameters Obtained from TGA Measurements for Neat PLA, STPLA, and STPLA/*x*AHP with Different AHP Contents under Nitrogen Atmosphere

sample code	$T_{0.05}$ (°C)	$T_{max,PLA}$ (°C)	$T_{max,EGMA}$ (°C)	$T_{max,AHP}$ (°C)	residue (%)
neat PLA	351	385			1.3
STPLA	360	385	469		4.0
STPLA/10AHP	349	386	469	345	6.4
STPLA/20AHP	348	386	475	345	17.4
STPLA/30AHP	341	386	472	342	24.6
STPLA/40AHP	339	386	472	341	29.5

Table 3. Thermal Stability Parameters Obtained from TGA Measurements for Neat PLA, STPLA, and STPLA/*x*AHP with Different AHP Contents under Air Atmosphere

sample code	$T_{0.05}$ (°C)	$T_{max,PLA}$ (°C)	$T_{max,EGMA}$ (°C)	$T_{max,AHP}$ (°C)	residue (%)
neat PLA	340	372			0
STPLA	349	375	446		3.9
STPLA/10AHP	339	371	455	339	9.2
STPLA/20AHP	339	375	457	338	19.0
STPLA/30AHP	336	373	461	336	28.6
STPLA/40AHP	332	367		336	33.5

DOI: 10.1021/acsomega.7b00162
ACS Omega 2017, 2, 1886−1895

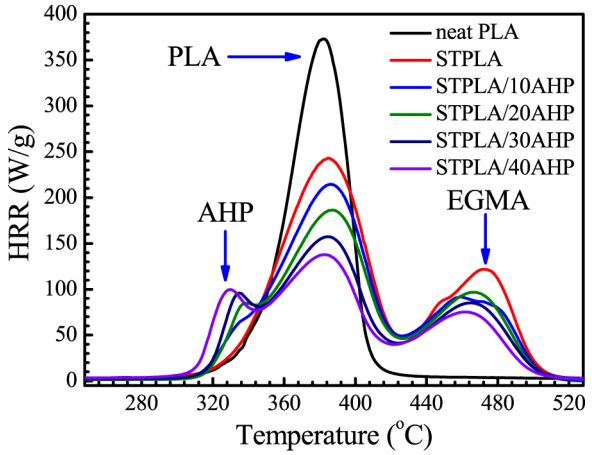

Figure 5. HRR curves obtained from MCC for neat PLA, STPLA, and STPLA/*x*AHP with different AHP contents.

with the value of 123 W/g can be seen at a higher temperature, which can be attributed to the contribution of the EGMA component in STPLA. Therefore, the reduction of PHRR of the PLA component in STPLA itself indicates reduced fire hazards due to the introduction of EGMA.

The changes of PHRR, THR, and temperature at PHRR as functions of AHP content for flame-retardant STPLA/*x*AHP with different AHP contents are collectively shown in Figure 6. The comparative changing trends of PHRR for PLA and EGMA follow similar decreases as the AHP content increases (Figure 6a) and the THR follows a similar decreasing trend (Figure 6b), implying that the presence of AHP can effectively reduce the fire hazards. The temperatures at PHRR for both PLA and EGMA components in the composites do not show obvious changes (Figure 6c), and PHRR at the lowest temperature is attributed to thermal degradation of the AHP component. Results from the MCC test illustrate that, besides AHP, the EGMA component also helps decrease fire hazards for the flame-retardant STPLA/*x*AHP.

The cone calorimeter is a useful bench-scale method for defining the flame-retardant property of materials in real-world fire conditions.[52] Therefore, the cone calorimeter was further applied to examine the influence of the AHP content on flammability of STPLA/*x*AHP. Figure 7 shows the HRR curves obtained from the cone calorimeter for neat PLA, STPLA, and STPLA/*x*AHP. The HRR curve is considered to be a powerful indicator for evaluating the fire hazardousness of materials by quantifying the fire size and fire growth rate from which the values of the time to ignition (TTI), PHRR, peak time of HRR (T_p), and THR can be extracted.[52] These values for neat PLA, STPLA, and STPLA/*x*AHP are listed in Table 4. As shown in Figure 7, neat PLA and STPLA burn quickly after an ignition and have relatively narrow peaks and high peak intensities, with the PHRR values as high as 1100 and 890 kW/m^2, respectively. The HRR curves for STPLA/*x*AHP become broadened and the peak intensities decrease as well. STPLA/10AHP has a PHRR of 440 kW/m^2 and STPLA/20AHP has an even lower PHRR value of 350 kW/m^2, and no further obvious reduction in PHRR can be found by further increasing the AHP content. For STPLA/*x*AHP, the THR values show a slight reduction as compared to those of neat PLA and STPLA. The TTI value for neat PLA is about 50 s, while that for STPLA/*x*AHP shifts to earlier times. As shown in the TGA and MCC results, the AHP component decomposes at an earlier time as compared with

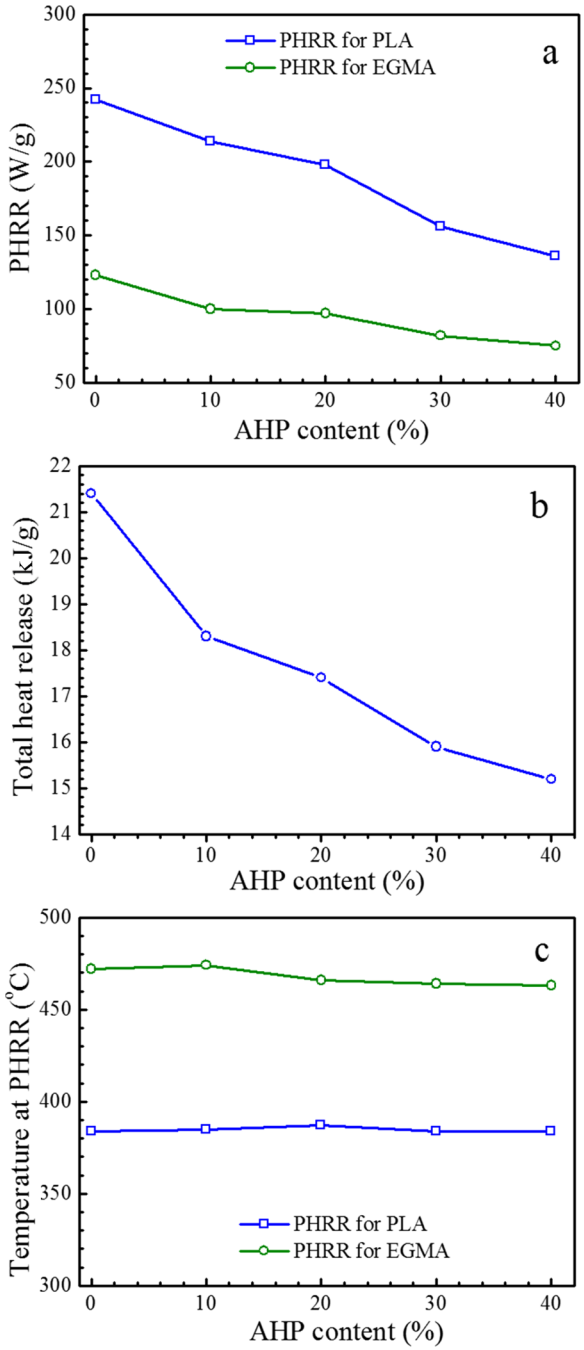

Figure 6. Changes in PHRR (a), THR (b), and temperature at PHRR (c) obtained from MCC as functions of the AHP content for flame-retardant STPLA/*x*AHP with different AHP contents.

PLA and EGMA, and PLA is sensitive to the acid species that result from the pyrolysis products of AHP, and thereby an addition of AHP catalyzes the degradation of PLA and reduces the TTI values.

2.5. Phase Separation Morphology Observed by PCOM. The phase separation morphology of STPLA (PLA/EGMA 80/20 blend) and the dispersion of AHP particles in the STPLA matrix for STPLA/*x*AHP were observed by using phase contrast optical microscopy (PCOM). The result is shown in Figure 8. Phase separation domains can be observed for STPLA (micrograph not shown here), indicating that the EGMA component is not fully miscible with the PLA matrix. However,

DOI: 10.1021/acsomega.7b00162
ACS Omega 2017, 2, 1886−1895

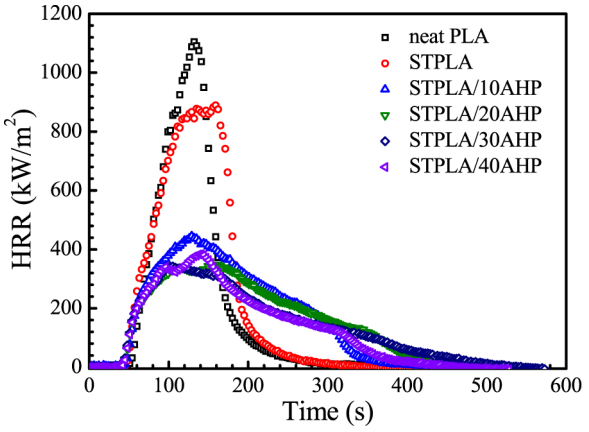

Figure 7. HRR curves as measured from cone calorimeter for neat PLA, STPLA, and STPLA/*x*AHP with different AHP contents.

Table 4. TTI, T_p, PHRR, and THR values for Neat PLA, STPLA, and STPLA/*x*AHP with Different AHP Contents

sample code	TTI (s)	T_p (s)	PHRR (kW/m^2)	THR (MJ/m^2)
neat PLA	50	130	1100	86
STPLA	46	160	890	95
STPLA/10AHP	45	130	440	81
STPLA/20AHP	44	160	350	79
STPLA/30AHP	36	100	340	75
STPLA/40AHP	30	140	380	69

due to obvious interfacial reactions between the EGMA and PLA components, the phase domain boundary is blurred and indistinct for STPLA. With the incorporation of AHP, phase separation can still be visible, as shown in Figure 8. For STPLA/10AHP and STPLA/20AHP, the flame-retardant AHP particles are relatively homogeneously dispersed in the STPLA matrix with no obviously large AHP particle agglomeration, whereas for STPLA/30AHP and STPLA/40AHP, large AHP particle agglomeration can be clearly seen, as pointed out by the blue arrows in Figure 8, which is responsible for deterioration of the mechanical property of STPLA/*x*AHP at these two highest AHP contents.

2.6. Fracture Surface and Char Residue Morphologies Observed by Scanning Electron Microscopy (SEM). The fracture surfaces of the notched Izod impact sample bars were examined by SEM, and the typical SEM micrographs for neat PLA, STPLA, and STPLA/20AHP are shown in Figure 9. A balance between the mechanical property and flame retardancy is required for material applications. As discussed in a previous section, STPLA/*x*AHP with the AHP content of 20 wt % achieves a sufficient balance between its mechanical property and flame retardancy. It can be seen from Figure 9a that neat PLA shows a smooth and almost featureless fracture surface without much deformations, indicating a typical brittle fracture behavior. The fracture surface of STPLA displays a rugged feature (Figure 9b), indicating that the PLA matrix experiences shear yielding during mechanical deformation, which can be induced by cavitation of the rubbery EGMA phase domains. With the incorporation of the AHP particles, the fracture surface of STPLA/20AHP still displays a rugged feature (Figure 9c), indicating a similar mechanical deformation mechanism for the composite. In addition, it can be seen from Figure 9c that some AHP particles insert into the STPLA matrix and certain voids can be found around these AHP particles, indicating poor adhesion between the AHP particles and STPLA matrix, which is responsible for the relative decrease in notched Izod impact strength as compared to that of STPLA.

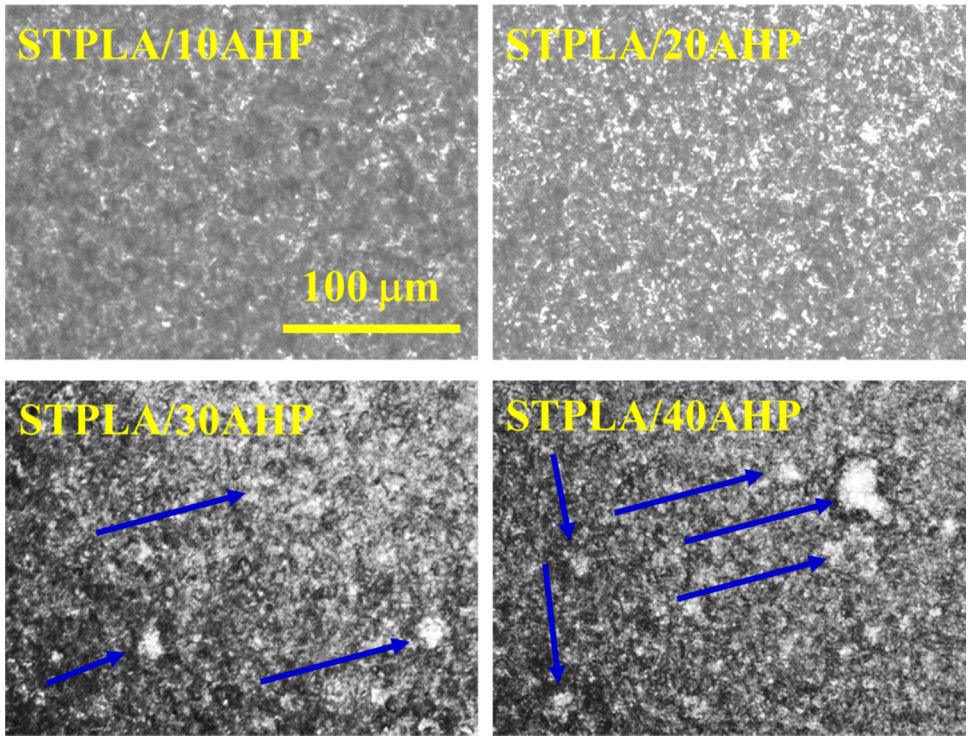

Figure 8. PCOM micrographs observed at 200 °C for STPLA/*x*AHP. The yellow scale bar represents 50 μm and is applied to all the micrographs. Large AHP particle agglomeration is illustrated by blue arrows.

DOI: 10.1021/acsomega.7b00162
ACS Omega 2017, 2, 1886−1895

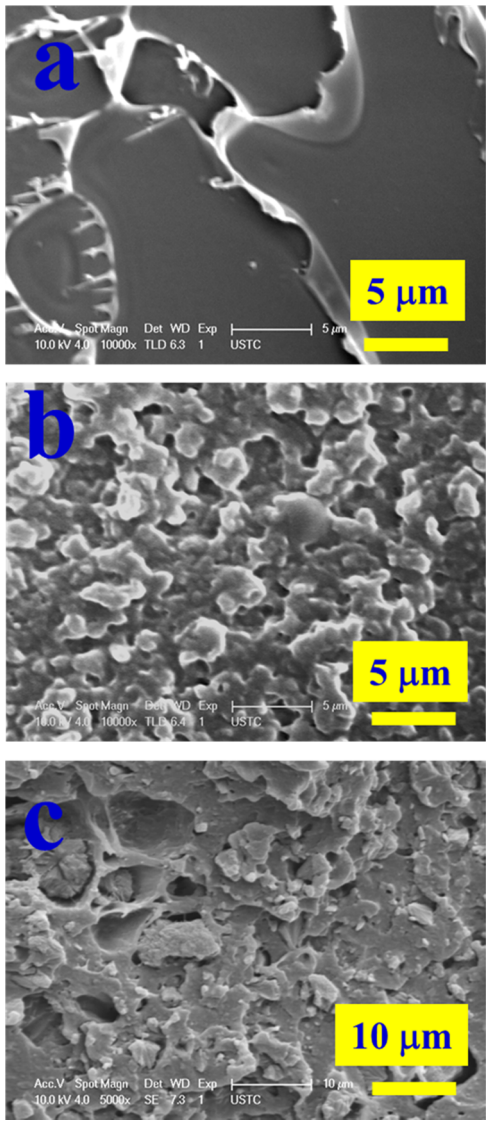

Figure 9. SEM micrographs taken on the fracture surfaces of the notched Izod impact sample bars for neat PLA (a), STPLA (b), and STPLA/20AHP (c).

Figure 10 shows the SEM micrographs of the char residues of STPLA/20AHP. A continuous char layer at the char surface is clearly seen in Figure 10a, which evidences the flame retardancy. When observed under high magnification as shown in Figure 10b, the char residue particles in the continuous layer look compact and dense with several sparse crater-like structures existing, which may have resulted from the thermally released gas products from the degradation of AHP. Overall, the SEM micrographs confirm sufficient flame retardancy for STPLA/20AHP.

3. CONCLUSIONS

In this work, supertough flame-resistant PLA composites were successfully prepared by using economically effective reactive melt blending approach. PLA and EGMA were reactively blended in the molten state as a polymer matrix with a mass ratio of 80/20, which provided the supertough mechanical property, coded as STPLA, and then the composites STPLA/*x*AHP were prepared with a continuous mixing with AHP as an effective flame retardant, where *x* represented the mass

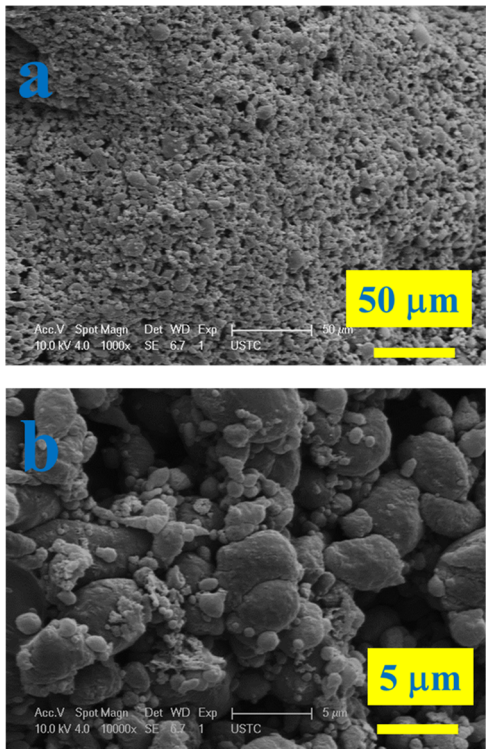

Figure 10. SEM micrographs at a low magnification (a) and a high magnification (b) for char residues after combustion of STPLA/20AHP.

contents of AHP relative to the mass of STPLA. Taking the optimal formula as a typical example, STPLA/20AHP successfully passed the UL-94 V0 rating in the UL-94 test, had an LOI value of 26.6% and showed an antidripping phenomenon, indicating its sufficient flame retardancy for application purpose; in the mechanical property aspect, STPLA/20AHP showed an elongation at break of 131% during the tensile test and a notched Izod impact strength of 22 kJ/m^2, nearly 23 and 12 times of that of neat PLA, respectively, reflecting its supertough mechanical property. TGA was applied to examine the thermal decomposition behavior, and MCC and cone calorimeter were further applied to examine the combustion property for STPLA/*x*AHP, which revealed the possible flame-retardant mechanisms. PCOM was used to observe the phase separation morphology and dispersion of AHP particles in the STPLA matrix, which indicated that the mechanical deformation mechanism of STPLA/*x*AHP was related to the interfacial layers formed during reactive blending and the degree of formation of heterogeneous AHP agglomeration. Finally, SEM was used to observe the fracture surfaces of the notched Izod impact sample bars and the surfaces of char residues after combustion for further understanding of the flame-retardant mechanism. In summary, the approach employed in this work might broaden the applications of PLA materials, which might release some environmental pressure.

4. EXPERIMENTAL SECTION

4.1. Materials. Commercially available PLA (Natureworks product PLA2003D) was purchased for this study. The PLA sample had a density of 1.24 g/cm^3 and a melt flow index of 6 g/10 min (210 °C, 2.16 kg). The chosen reactive elastomer (LOTADER; AX8900, Arkema) was EGMA random terpol-

DOI: 10.1021/acsomega.7b00162
ACS Omega 2017, 2, 1886−1895

ymer (EGMA). The methyl acrylate and glycidyl methacrylate contents in EGMA were 24 and 8%, respectively. The melt flow index of EGMA was 6 g/10 min (190 °C, 2.16 kg). AHP as a flame retardant was bought from Qingyuan RGDC Chemicals Ltd., China.

4.2. Reactive Melt Blending. PLA and AHP were dried at 60 °C, and EGMA was dried at 40 °C under vacuum for 12 h prior to melt blending. PLA and EGMA with a mass ratio of 80/20 were mixed at a rotor speed of 80 rpm and 200 °C for 8 min by using an XSS-300 torque rheometer. Subsequently, AHP of certain amounts was added in for another 4 min mixing. In this study, the PLA/EGMA 80/20 blend was denoted as the polymer matrix and AHP mass contents were chosen to be 10, 20, 30, and 40 wt %, relative to the mass of the PLA/EGMA 80/20 blend. For simplicity, the PLA/EGMA 80/20 blend is coded as STPLA (supertough PLA), and the PLA composites, with addition of AHP of various amounts, are coded as STPLA/*x*AHP, where *x* indicates the mass contents of AHP in percentage.

4.3. Mechanical Property Testing. STPLA and STPLA/*x*AHP were hot pressed at 200 °C under a pressure of 10 MPa for 5 min into sheets with a thickness of about 1 mm, using a homemade vacuum laminator and then were quenched to room temperature. Dumbbell-shaped samples were punched out from the molded sheets for mechanical tensile property test. The tensile property was measured at room temperature according to ASTM 638 by using an electronic universal tensile test machine (Suns, Shenzhen, China) at a crosshead speed of 10 mm/min. The notched Izod impact strength test was performed by using an XJUD-5.5 pendulum impact tester (JinJian-test, China). The size of the rectangular specimen was 100 × 10 × 3 mm^3, with a 45° V-shaped notch (upper radius of 0.25 mm and depth of 2 mm). The average values from measurements on five specimens were used for data analysis.

4.4. Flame Retardancy Testing. LOI measurements were carried out using an HC-2 oxygen index meter (Nanjing Jiangning Analysis Instrument Ltd., China) according to ASTM D2863-97. The size of the specimens was 130 × 6.5 × 3.2 mm^3. The UL-94 vertical tests were carried out using a CZF-1 type instrument (made in china). The size of the specimens was 130 × 13 × 3 mm^3. In the UL-94 tests, the specimens were vertically exposed to a Bunsen burner flame for a period of 10 s. If the flame was extinguished, another period of 10 s was employed. The UL-94 rating for STPLA/*x*AHP was determined according to ANSL/UL-94-2009.

4.5. Thermal Stability Property Measurement. A Q5000 IR thermogravimetric analyzer (TA Instruments) was used for the TGA. Alumina crucibles were used. The masses of the samples were about 5−10 mg. The measurement temperature ranged from room temperature to 600 °C, and the heating rate was 20 °C/min. The measurements were performed under nitrogen and air atmosphere, respectively. The temperature at which the original sample mass of 5% was lost was defined as the onset decomposition temperature. The temperature with the maximum mass loss rate was defined as T_{max} for each component in the sample.

4.6. Combustion Property Testing. The combustion property of the samples was probed by using MCC (model FAA-PCFC; Fire Testing Technology); 4−6 mg of each sample were used. The sample was heated from 100 to 650 °C at 1 °C/s in a nitrogen stream, with a flow rate of 8 × 10^{-5} m^3/min. Prior to flowing into a 900 °C combustion furnace, the volatile anaerobic thermal degradation products in the nitrogen stream were mixed with an oxygen stream with a flow rate of 2 × 10^{-5} m^3/min. The cone calorimeter test was performed on a cone calorimeter (Fire Testing Technology, U.K.) according to ASTM E1354/ISO 5660. The size of the specimens was 100 × 100 × 3 mm^3. Each specimen was wrapped in an aluminum foil and exposed horizontally to a 35 kW/m^2 external heat flux.

4.7. Phase Separation Observation by PCOM. To examine the miscibility between PLA and EGMA in STPLA in the melt state and dispersion of AHP in the STPLA matrix for STPLA/*x*AHP, PCOM (Olympus BX51) was applied to observe the phase separation morphology. The film samples of the blend and composites were melted at 200 °C for 2 min before the PCOM micrographs were taken.

4.8. Fracture Surface and Residue Observation by SEM. To evaluate the mechanical deformation and flame-retardant mechanisms, the impact fractured surfaces of the samples and char residues after combustion of STPLA and STPLA/20AHP were sputter-coated with gold and then the surface morphologies were examined by using a field-emission scanning electron microscope (SEM, FEI, Sirion200).

■ ASSOCIATED CONTENT

Supporting Information

The Supporting Information is available free of charge on the ACS Publications website at DOI: 10.1021/acsomega.7b00162.

HRR and THR curves obtained from the cone calorimeter tests for neat PLA, EGMA, and STPLA (PDF)

■ AUTHOR INFORMATION

Corresponding Author

*E-mail: zgwang2@ustc.edu.cn. Tel: +86 0551-63607703. Fax: +86 0551-63607703.

ORCID

Zhigang Wang: 0000-0002-6090-3274

Author Contributions

†S.L. and L.D. contributed equally to this work.

Notes

The authors declare no competing financial interest.

■ ACKNOWLEDGMENTS

Z.G.W. acknowledges financial support from the National Natural Science Foundation of China (Grant Nos. 51473155 and 51673183). The project is also supported by the Open Research Fund of State Key Laboratory of Polymer Physics and Chemistry, Changchun Institute of Applied Chemistry, Chinese Academy of Sciences. The authors thank Prof. Tao Tang of the Changchun Institute of Applied Chemistry, Chinese Academy of Sciences, for his kind help in providing the use of the MCC facility in his group.

■ REFERENCES

(1) Drumright, R. E.; Gruber, P. R.; Henton, D. E. Polylactic Acid Technology. *Adv. Mater.* **2000**, *12*, 1841−1846.

(2) Gross, R. A.; Kalra, B. Biodegradable Polymers for the Environment. *Science* **2002**, *297*, 803−807.

(3) Jamshidian, M.; Tehrany, E. A.; Imran, M.; Jacquot, M.; Desobry, S. Poly-Lactic Acid: Production, Applications, Nanocomposites, and Release Studies. *Compr. Rev. Food Sci. Food Saf.* **2010**, *9*, 552−571.

(4) Auras, R. A.; Lim, L. T.; Selke, S. E.; Tsuji, H. *Poly (Lactic Acid): Synthesis, Structures, Properties, Processing, and Applications*; John Wiley & Sons, 2011; pp 457−467.

DOI: 10.1021/acsomega.7b00162
ACS Omega 2017, 2, 1886−1895

(5) Sin, L. T.; Rahmat, A. R.; Rahman, W. A. *Poly (Lactic Acid): PLA Biopolymer Technology and Applications*; William Andrew, 2012; pp 33−56.
(6) Liu, H.; Zhang, J. Research Progress in Toughening Modification of Poly (Lactic Acid). *J. Polym. Sci., Part B: Polym. Phys.* **2011**, *49*, 1051−1083.
(7) Bourbigot, S.; Fontaine, G. Flame Retardancy of Polylactide: An Overview. *Polym. Chem.* **2010**, *1*, 1413−1422.
(8) Song, Y. P.; Wang, D. Y.; Wang, X. L.; Lin, L.; Wang, Y. Z. A Method for Simultaneously Improving the Flame Retardancy and Toughness of PLA. *Polym. Adv. Technol.* **2011**, *22*, 2295−2301.
(9) Chow, W. S.; Teoh, E. L. Flexible and Flame Resistant Poly (Lactic Acid)/Organomontmorillonite Nanocomposites. *J. Appl. Polym. Sci.* **2015**, *132*, 1−11.
(10) Wei, L. L.; Wang, D. Y.; Chen, H. B.; Chen, L.; Wang, X. L.; Wang, Y. Z. Effect of A Phosphorus-Containing Flame Retardant on the Thermal Properties and Ease of Ignition of Poly (Lactic Acid). *Polym. Degrad. Stab.* **2011**, *96*, 1557−1561.
(11) Liu, X. Q.; Wang, D. Y.; Wang, X. L.; Chen, L.; Wang, Y. Z. Synthesis of Organo-Modified α-Zirconium Phosphate and its Effect on the Flame Retardancy of IFR Poly (Lactic Acid) Systems. *Polym. Degrad. Stab.* **2011**, *96*, 771−777.
(12) Yuan, X. Y.; Wang, D. Y.; Chen, L.; Wang, X. L.; Wang, Y. Z. Inherent Flame Retardation of Bio-Based Poly (Lactic Acid) by Incorporating Phosphorus Linked Pendent Group into the Backbone. *Polym. Degrad. Stab.* **2011**, *96*, 1669−1675.
(13) Mauldin, T. C.; Zammarano, M.; Gilman, J. W.; Shields, J. R.; Boday, D. J. Synthesis and Characterization of Isosorbide-Based Polyphosphonates as Biobased Flame-Retardants. *Polym. Chem.* **2014**, *5*, 5139−5146.
(14) Murariu, M.; Bonnaud, L.; Yoann, P.; Fontaine, G.; Bourbigot, S.; Dubois, P. New Trends in Polylactide (PLA)-Based Materials: "Green" PLA-Calcium Sulfate (Nano) Composites Tailored with Flame Retardant Properties. *Polym. Degrad. Stab.* **2010**, *95*, 374−381.
(15) Akbari, A.; Majumder, M.; Tehrani, A. Polylactic Acid (PLA) Carbon Nanotube Nanocomposites. In *Handbook of Polymer Nanocomposites. Processing, Performance and Application*; Springer, 2015; pp 283−297.
(16) Fox, D. M.; Lee, J.; Citro, C. J.; Novy, M. Flame Retarded Poly (Lactic Acid) Using POSS-Modified Cellulose. 1. Thermal and Combustion Properties of Intumescing Composites. *Polym. Degrad. Stab.* **2013**, *98*, 590−596.
(17) Gao, Y.; Wu, J.; Wang, Q.; Wilkie, C. A.; O'Hare, D. Flame Retardant Polymer/Layered Double Hydroxide Nanocomposites. *J. Mater. Chem. A* **2014**, *2*, 10996−11016.
(18) Bocz, K.; Domonkos, M.; Igricz, T.; Kmetty, Á.; Bárány, T.; Marosi, G. Flame Retarded Self-Reinforced Poly (Lactic Acid) Composites of Outstanding Impact Resistance. *Composites, Part A* **2015**, *70*, 27−34.
(19) Stoclet, G.; Sclavons, M.; Lecouvet, B.; Devaux, J.; Van Velthem, P.; Boborodea, A.; Bourbigot, S.; Sallem-Idrissi, N. Elaboration of Poly (Lactic Acid)/Halloysite Nanocomposites by Means of Water Assisted Extrusion: Structure, Mechanical Properties and Fire Performance. *RSC Adv.* **2014**, *4*, 57553−57563.
(20) Song, L.; Xuan, S.; Wang, X.; Hu, Y. Flame Retardancy and Thermal Degradation Behaviors of Phosphate in Combination with POSS in Polylactide Composites. *Thermochim. Acta* **2012**, *527*, 1−7.
(21) Qian, Y.; Wei, P.; Jiang, P.; Li, Z.; Yan, Y.; Ji, K. Aluminated Mesoporous Silica as Novel High-Effective Flame Retardant in Polylactide. *Compos. Sci. Technol.* **2013**, *82*, 1−7.
(22) Wang, D. Y.; Song, Y. P.; Lin, L.; Wang, X. L.; Wang, Y. Z. A Novel Phosphorus-Containing Poly (Lactic Acid) Toward its Flame Retardation. *Polymer* **2011**, *52*, 233−238.
(23) Zhan, J.; Song, L.; Nie, S.; Hu, Y. Combustion Properties and Thermal Degradation Behavior of Polylactide with an Effective Intumescent Flame Retardant. *Polym. Degrad. Stab.* **2009**, *94*, 291−296.
(24) Réti, C.; Casetta, M.; Duquesne, S.; Bourbigot, S.; Delobel, R. Flammability Properties of Intumescent PLA Including Starch and Lignin. *Polym. Adv. Technol.* **2008**, *19*, 628−635.
(25) Nishida, H.; Fan, Y.; Mori, T.; Oyagi, N.; Shirai, Y.; Endo, T. Feedstock Recycling of Flame-Resisting Poly (Lactic Acid)/Aluminum Hydroxide Composite to L, L-lactide. *Ind. Eng. Chem. Res.* **2005**, *44*, 1433−1437.
(26) Murariu, M.; Dechief, A. L.; Bonnaud, L.; Paint, Y.; Gallos, A.; Fontaine, G.; Bourbigot, S.; Dubois, P. The Production and Properties of Polylactide Composites Filled with Expanded Graphite. *Polym. Degrad. Stab.* **2010**, *95*, 889−900.
(27) Feng, J. X.; Su, S. P.; Zhu, J. An Intumescent Flame Retardant System Using β-Cyclodextrin as A Carbon Source in Polylactic Acid (PLA). *Polym. Adv. Technol.* **2011**, *22*, 1115−1122.
(28) Bai, H.; Bai, D.; Xiu, H.; Liu, H.; Zhang, Q.; Wang, K.; Deng, H.; Chen, F.; Fu, Q.; Chiu, F.-C. Towards High-Performance Poly(L-Lactide)/Elastomer Blends with Tunable Interfacial Adhesion and Matrix Crystallization via Constructing Stereocomplex Crystallites at the Interface. *RSC Adv.* **2014**, *4*, 49374−49385.
(29) Wang, Y.; Wei, Z.; Leng, X.; Shen, K.; Li, Y. Highly Toughened Polylactide with Epoxidized Polybutadiene by in-situ Reactive Compatibilization. *Polymer* **2016**, *92*, 74−83.
(30) Wu, M.; Wu, Z.; Wang, K.; Zhang, Q.; Fu, Q. Simultaneous the Thermodynamics Favorable Compatibility and Morphology to Achieve Excellent Comprehensive Mechanics in PLA/OBC Blend. *Polymer* **2014**, *55*, 6409−6417.
(31) Fang, H.; Jiang, F.; Wu, Q. H.; Ding, Y. S.; Wang, Z. G. Supertough Polylactide Materials Prepared through in situ Reactive Blending with PEG-based Diacrylate Monomer. *ACS Appl. Mater. Interfaces* **2014**, *6*, 13552−13563.
(32) Oyama, H. T. Super-tough Poly (Lactic Acid) Materials: Reactive Blending with Ethylene Copolymer. *Polymer* **2009**, *50*, 747−751.
(33) Liu, H.; Song, W.; Chen, F.; Guo, L.; Zhang, J. Interaction of Microstructure and Interfacial Adhesion on Impact Performance of Polylactide (PLA) Ternary Blends. *Macromolecules* **2011**, *44*, 1513−1522.
(34) Liu, H.; Chen, F.; Liu, B.; Estep, G.; Zhang, J. Super Toughened Poly (Lactic Acid) Ternary Blends by Simultaneous Dynamic Vulcanization and Interfacial Compatibilization. *Macromolecules* **2010**, *43*, 6058−6066.
(35) Dong, W.; Jiang, F.; Zhao, L.; You, J.; Cao, X.; Li, Y. PLLA Microalloys versus PLLA Nanoalloys: Preparation, Morphologies, and Properties. *ACS Appl. Mater. Interfaces* **2012**, *4*, 3667−3675.
(36) Liu, G. C.; He, Y. S.; Zeng, J. B.; Li, Q. T.; Wang, Y. Z. Fully Biobased and Supertough Polylactide-Based Thermoplastic Vulcanizates Fabricated by Peroxide-Induced Dynamic Vulcanization and Interfacial Compatibilization. *Biomacromolecules* **2014**, *15*, 4260−4271.
(37) Dong, W.; Wang, H.; He, M.; Ren, F.; Wu, T.; Zheng, Q.; Li, Y. Synthesis of Reactive Comb Polymers and Their Applications as A Highly Efficient Compatibilizer in Immiscible Polymer Blends. *Ind. Eng. Chem. Res.* **2015**, *54*, 2081−2089.
(38) Yang, X.; Clénet, J.; Xu, H.; Odelius, K.; Hakkarainen, M. Two Step Extrusion Process: From Thermal Recycling of PHB to Plasticized PLA by Reactive Extrusion Grafting of PHB Degradation Products onto PLA Chains. *Macromolecules* **2015**, *48*, 2509−2518.
(39) Williams, C.; Hillmyer, M. Polymers from Renewable Resources: A Perspective for A Special Issue of Polymer Reviews. *Polym. Rev.* **2008**, *48*, 1−10.
(40) Lim, L. T.; Auras, R.; Rubino, M. Processing Technologies for Poly(Lactic Acid). *Prog. Polym. Sci.* **2008**, *33*, 820−852.
(41) Anderson, K.; Schreck, K.; Hillmyer, M. Toughening Polylactide. *Polym. Rev.* **2008**, *48*, 85−108.
(42) Yu, L.; Dean, K.; Li, L. Polymer Blends and Composites from Renewable Resources. *Prog. Polym. Sci.* **2006**, *31*, 576−602.
(43) Zhang, K.; Nagarajan, V.; Misra, M.; Mohanty, A. K. Supertoughened Renewable PLA Reactive Multiphase Blends System: Phase Morphology and Performance. *ACS Appl. Mater. Interfaces* **2014**, *6*, 12436−12448.

DOI: 10.1021/acsomega.7b00162
ACS Omega 2017, 2, 1886−1895

(44) Zhao, X.; Lv, L.; Pan, B.; Zhang, W.; Zhang, S.; Zhang, Q. Polymer-Supported Nanocomposites for Environmental Application: A Review. *Chem. Eng. J.* **2011**, *170*, 381−394.
(45) Dong, W.; Jiang, F.; Zhao, L.; You, J.; Cao, X.; Li, Y. PLLA Microalloys versus PLLA Nanoalloys: Preparation, Morphologies, and Properties. *ACS Appl. Mater. Interfaces* **2012**, *4*, 3667−3675.
(46) Mélo, T. J. A.; Araújo, E. M.; Brito, G. F.; Agrawal, P. Development of Nanocomposites from Polymer Blends: Effect of Organoclay on the Morphology and Mechanical Properties. *J. Alloys Compd.* **2014**, *615*, S389−S391.
(47) Brito, G. F.; Agrawal, P.; Araújo, E. M.; Mélo, T. J. A. Effect of Combining Ethylene/Methyl Acrylate/Glycidyl Methacrylate Terpolymer and An Organoclay on the Toughening of Poly(Lactic Acid). *Polym. Eng. Sci.* **2014**, *54*, 1922−1930.
(48) Braun, U.; Schartel, B.; Fichera, M. A.; Jäger, C. Flame Retardancy Mechanisms of Aluminium Phosphinate in Combination with Melamine Polyphosphate and Zinc Borate in Glass-Fibre Reinforced Polyamide 6,6. *Polym. Degrad. Stab.* **2007**, *92*, 1528−1545.
(49) Yang, W.; Song, L.; Hu, Y.; Lu, H.; Yuen, R. K. K. Enhancement of Fire Retardancy Performance of Glass-Fibre Reinforced Poly(Ethylene Terephthalate) Composites with the Incorporation of Aluminum Hypophosphite and Melamine Cyanurate. *Composites, Part B* **2011**, *42*, 1057−1065.
(50) Tang, G.; Wang, X.; Xing, W.; Zhang, P.; Wang, B.; Hong, N.; Yang, W.; Hu, Y.; Song, L. Thermal Degradation and Flame Retardance of Biobased Polylactide Composites Based on Aluminum Hypophosphite. *Ind. Eng. Chem. Res.* **2012**, *51*, 12009−12016.
(51) Lyon, R. E.; Walters, R. N.; Stoliarov, S. I. Screening Flame Retardants for Plastics Using Microscale Combustion Calorimetry. *Polym. Eng. Sci.* **2007**, *47*, 1501−1510.
(52) Gilman, J. Flammability and Thermal Stability Studies of Polymer Layered-Silicate (Clay) Nanocomposites. *Appl. Clay Sci.* **1999**, *15*, 31−49.

DOI: 10.1021/acsomega.7b00162
ACS Omega 2017, 2, 1886−1895